

Two-stage electron acceleration by 3D collisionless guide field magnetic reconnection

P. A. Muñoz^{a)} and J. Büchner

Max-Planck-Institut für Sonnensystemforschung, D-37077 Göttingen, Germany^{b)}

We report a new two-stage mechanism of electron acceleration near X-lines of 3D collisionless guide-field magnetic reconnection in the non-relativistic regime typical, e.g., for stellar coronae. We found that after electrons are first pre-accelerated by magnetic-field-aligned (parallel) electric fields, reconnection becomes nonlinearly enhanced. At the nonlinear stage of 3D guide-field magnetic reconnection, electric and magnetic fields become filamentary structured due to streaming instabilities. This filamentation causes an additional curvature-driven electron acceleration in the guide-field direction. As a result, part of the accelerated electron spectra becomes a power law with a spectral index of ~ -1.6 . This non-linear reconnection acceleration is relevant for the formation of energetic electron distributions out of a thermal distribution.

I. Introduction

One of the unsolved puzzles in the Universe is the acceleration of electrons to high energies in a wide variety of astrophysical objects, as remotely detected by their high-frequency electromagnetic radiation, e.g., of hard X-rays from the Sun's chromosphere during solar flares^{1,2}, or directly observed by in-situ spacecrafts measurements like by the ongoing MMS mission³. The latter also provides the typical plasma and fields conditions at the acceleration sites⁴. Common for those observations is the presence of current sheets (CSs) and magnetic reconnection through them. Reconnection can, in principle, accelerate electrons at the expense of the annihilation of magnetic flux and energy⁵.

Mechanisms of efficient acceleration of non-relativistic electrons by guide-field magnetic reconnection are, however, still not clear. They were investigated, e.g., by test particle calculations using prescribed reconnection fields usually obtained by MHD simulations. They revealed effective electron acceleration mainly by magnetic-field-aligned (parallel) reconnection electric fields (E_{\parallel}) both near single⁶ and multiple X-lines⁷, in stochastic CSs⁸, in turbulent fields⁹, and also via a two-stage energization process¹⁰. Test particle calculations, however, do not take into account the feedback of the energized electrons to the plasma. In addition, they usually overestimate the electron acceleration since the parallel electric fields obtained by ad-hoc assumed “anomalous” resistivity, or numerical effects (resistivity), are much larger than in collisionless astrophysical plasmas^{9,11}. To avoid assumptions about “anomalous” resistivity, or the usually high and not well controlled numerical resistivity, self-consistent kinetic models can be used which are, however, limited to relatively small spatial scales. Fully-kinetic PIC-code simulations of already relativistic electron-proton plasmas revealed effective electron acceleration by reconnection in 2D-^{12,13} and 3D-¹⁴ configurations as well as for

relativistic pair plasmas^{15,16}. Power-law energy spectra were found in these strongly magnetically dominated plasmas, where the energy available for acceleration is orders of magnitude larger than the plasma rest energy. For non-relativistic electron-proton plasmas, PIC-code investigations revealed so far only a weak electron energization by the reconnection electric field near X-lines in 2D configurations, possibly enhanced by mechanisms such as surfing and E_{\parallel} in the separatrixes^{17,18}. First order Fermi-type acceleration was detected in contracting magnetic islands (plasmoids) of long CSs in 2D^{19,20} and more efficiently in 3D configurations²¹. However, power-law energy spectra were hardly found. Stochastic Fermi acceleration due to the interaction of multiple magnetic islands was observed in the solar wind²² and reproduced in simulations of turbulent reconnecting plasmas^{23,24}. Fermi acceleration is, unfortunately, suppressed in strong guide-field (low plasma- β) magnetic reconnection. However, the problem of non-relativistic electron acceleration in guide field reconnection is critical to understand the observed X-ray spectra in solar and other stellar coronae, which require electrons out of a thermal distribution.

All the previous research did not, however, take into account the influence of the nonlinear evolution of 3D guide-field magnetic reconnection, which can cause a filamentation in the third dimension. We show that the filamentation in strong guide field (B_g , larger than the asymptotic, upstream, reconnection magnetic field $B_{\infty y}$) reconnection causes a so far unknown, second-stage of electron acceleration which generates power-law electron spectra even at single X-lines.

II. Method

We describe the nonlinear evolution of guide-field reconnection and the consequent 3D structure formation by fully-kinetic, relativistic PIC-code simulations using the code ACRONYM²⁵. To allow periodic boundary conditions in all three directions, we initialize two force-free equilibrium sheets of currents flowing in opposite directions and sufficiently separated, avoiding their interaction²⁶. We carried out 3D kinetic simulations with various parameters, out of which we illustrate our findings with results obtained for: an ion-electron mass ra-

^{a)} Electronic mail: munozp@mps.mpg.de

^{b)} Max-Planck/Princeton Center for Plasma Physics

tio $m_i/m_e = 100$, equal electron and ion temperatures $T_i = T_e$, a plasma beta $\beta_e = \beta_i = 2\mu_0 n_0 k_B T_i / B_T^2 = 0.08$, a ratio of the electron thermal speed to the speed of light of $v_{th,e}/c = 0.1$ and a relative guide field strength $b_g = B_g/B_{\infty y} = 2$. $B_T = B_{\infty y} \sqrt{1 + b_g^2}$ is the initially constant total magnetic field and the CS half-width is $L = 0.25 d_i$, where $d_i = c/\omega_{pi}$ is the ion inertial length and ω_{pi} is the ion plasma frequency. The initial ion and electron number densities are constant and equal ($n_i = n_e = n_0$). All other parameters and quantities can be obtained from the above given. Absolute values can be deduced by choosing the electron plasma frequency or density for the plasmas of interest (solar corona, solar wind, Earth's magnetosphere, etc).

In the PIC simulation, the simulation box $L_x \times L_y \times L_z$ covers a physical domain $4 d_i \times 8 d_i \times 16 d_i$. The numerical mesh is spanned over $256 \times 512 \times 1024$ grid points. We intentionally choose a simulation domain short enough in the y -direction to avoid island formation and to investigate two-stage electron acceleration at a single X-line. The plasma is represented by 200 macro-particles per cell (PPC; 100 per specie), which corresponds to a total of $2.7 \cdot 10^{10}$ particles in the simulation box. To verify the convergence of our results, we ran simulations with smaller and larger number of PPC. We found that only for less than 25 PPC, numerical collisions due to the PIC shot noise slow down the particles, causing numerical heating instead of electron acceleration²⁷. Finally, reconnection is triggered by a 3D perturbation of the magnetic field narrowly localized in the current direction (z) and with a long (most unstable) tearing-Eigenmode wavelength in the y -direction.

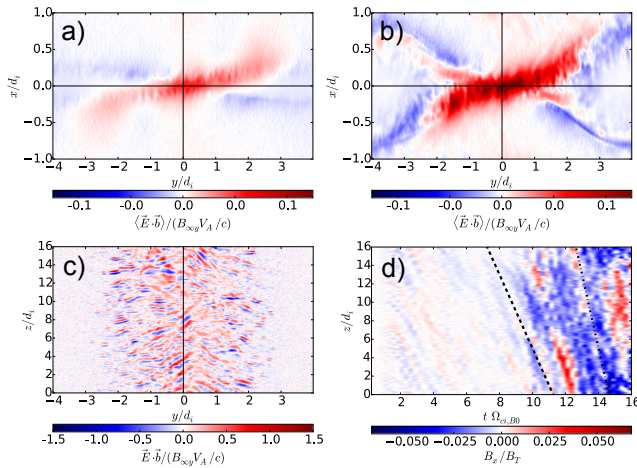


Figure 1. a) and b) Spatial distribution of $\langle E_{\parallel} \rangle$, the parallel electric field $E_{\parallel}(x, y)$ averaged over z , a) at $t = 10 \Omega_{ci}^{-1}$ and b) at $t = 13.5 \Omega_{ci}^{-1}$. c) Spatial distribution of $E_{\parallel}(y, z)$ in the CS central plane ($x = 0$) at $t = 13.5 \Omega_{ci}^{-1}$. d) Temporal evolution of the magnetic perturbations B_x along z ($x = y = 0$).

III. Two-stage acceleration

In three-dimensions a local perturbation causes a reconnection wave of a narrow quasi-2D reconnection in the plane perpendicular to the guide field, propagating in the guide-field direction. Figs. 1a)-b) show the resulting $\langle E_{\parallel} \rangle$, the parallel electric field E_{\parallel} averaged over the z direction in the plane $x - y$, at two characteristic times: at the end of the linear growth of reconnection ($t = 10 \Omega_{ci}^{-1}$) and in the middle of the nonlinear evolution ($t = 13.5 \Omega_{ci}^{-1}$). As usual, all PIC-quantities are time-averaged over $0.1 \Omega_{ci}^{-1}$ to remove the high-frequency PIC shot noise. The maximum $\langle E_{\parallel} \rangle$ grows as the reconnection rate, becoming $\langle E_{\parallel} \rangle = 0.08 E_0$ at $t = 10 \Omega_{ci}^{-1}$ and $0.15 E_0$ at $t = 13.5 \Omega_{ci}^{-1}$, respectively ($E_0 = V_A B_{\infty y}$ and V_A is the Alfvén speed on $B_{\infty y}$). During the linear evolution of reconnection, E_{\parallel} only mildly accelerates electrons without generating an energetic electron population or power-law spectra. Further the CS thins down, developing streaming and shear-flow-driven instabilities. These instabilities induce plasma waves which at their nonlinear stage cause a filamentation of E_{\parallel} and of the magnetic field in the guide-field direction z (see Muñoz and Büchner²⁸ for details about the evolution of the instabilities and the turbulence associated to them). Fig. 1c) shows the structure of $E_{\parallel}(y, z)$ in the central plane $x = 0$ (the CS center) at $t = 13.5 \Omega_{ci}^{-1}$. The signs of $E_{\parallel}(y, z)$ alternate (red/blue colors). The maximum absolute value of the parallel electric field is $|E_{\parallel, max}| = 1.5 E_0$, exceeding the average parallel electric field $\langle E_{\parallel} \rangle$ by a factor of ten. The work of the electromagnetic field on the particles ($\vec{j} \cdot \vec{E}$) and the associated dissipation are similarly structured (not shown here). This structure formation was already obtained before by PIC-code simulations near X-lines^{29,30} and separatrices of reconnection^{31,32} and found in the Earth's magnetosphere^{33,34}.

The evolution of the structure formation is illustrated by Fig. 1d), showing the magnetic field perturbation $B_x(z)$ along z for $x = y = 0$. The slopes of the dashed and dotted lines correspond to the initial (current-carrying) electron drift speed ($V_{De} \sim 4 V_A$) and twice that value, respectively. The filamentary structures propagate at the instantaneous electron drift speed, which increases due to the CS thinning, reaching a speed of $8 V_A$ at $t = 13.5 \Omega_{ci}^{-1}$. This spreading of reconnection was previously obtained also by two-fluid investigations³⁵, in experiments³⁶, in Hall-code³⁷, EMHD-code³⁸ and fully-kinetic CSs simulations^{39,40}. Reconnection spreads with the fastest speed between the electron drift ($4 V_A$, our case) and the speed of shear Alfvén waves propagating along the guide field ($2 V_A$).

Contributions to the electron acceleration can be characterized by the equations of the guiding-center motion when the electrons are fully magnetized, i.e., when the electron gyroradius stays smaller than the typical spatial scales of magnetic field variation. Indeed, the maximum electron gyroradius always satisfies this condition, the κ parameter^{41,42} (ratio of the curvature radius of magnetic

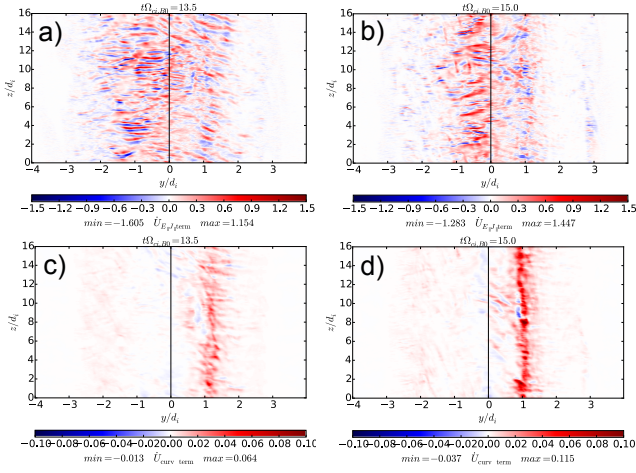


Figure 2. Electron energy change rate in the plane $y - z$ slightly off the center ($x = -0.1d_i$). Shown are the contributions of the first two terms of Eq. 1. Top row: $E_{\parallel}J_{\parallel}$ due to parallel electric fields at a) $t = 13.5\Omega_{ci}^{-1}$ and b) $t = 15\Omega_{ci}^{-1}$. Bottom row: Energy change by curvature-driven acceleration at c) $t = 13.5\Omega_{ci}^{-1}$ and d) $t = 15\Omega_{ci}^{-1}$.

field lines and electron gyroradius) is always above 10. Hence, changes of the electron energy can be quantified as^{20,43}:

$$\frac{dU}{dt} = E_{\parallel}J_{\parallel} + \left(p_{e,\parallel} + m_en_e u_{e,\parallel}^2\right) \vec{u}_{\vec{E}} \cdot \vec{\kappa} \quad (1) \\ + \frac{p_{e,\perp}}{B} \left(\frac{\partial B}{\partial t} + \vec{u}_{\vec{E}} \cdot \vec{\nabla} B\right).$$

Here U is the electron kinetic energy density, $\vec{u}_{\vec{E}}$ is the $\vec{E} \times \vec{B}$ drift speed, $p_{e,\parallel}/p_{e,\perp}$ are the parallel/perpendicular components of the electron pressure, $u_{e,\parallel}$ is the parallel electron bulk flow velocity and $\vec{\kappa} = (\vec{B}/B) \cdot \vec{\nabla}(\vec{B}/B)$ is the curvature of the magnetic field lines, a vector different from the aforementioned curvature parameter κ . The first term on the right-hand side (r.h.s.) of Eq. (1) describes the effect of parallel electric fields, the second is due to magnetic field curvature $\vec{\kappa}$. The third term is due to magnetic field inhomogeneities.

Figs. 2 shows the spatial distribution of the main contributions to the acceleration of all electrons (top and bottom rows) in a plane $y - z$ slightly off the center ($x = -0.1d_i$) at two different times. The contribution of the third term in the r.h.s. of Eq. (1) is not shown because it is always negligible, an order of magnitude smaller than the other two terms. In the Figures, the change of the electron energy density dU/dt is normalized to E_0J_0 , where $J_0 = en_e v_{th,e}$. Panels a)-b) and c)-d) in Fig. 2 clearly show that the parallel electric field term locally energizes electrons more efficiently than the curvature-driven acceleration. But on average, the latter energizes the electrons more efficiently. The maximum normalized energy gain due to the curvature term is $\dot{U}_{\text{curv,term}} \sim 0.06$ at $t = 13.5\Omega_{ci}^{-1}$, increasing up to

$\dot{U}_{\text{curv,term}} \sim 0.11$ at $t = 15\Omega_{ci}^{-1}$, reached near $y \sim 1d_i$ and always adding up. The net energy gain by the parallel electric fields $\dot{U}_{E_{\parallel}J_{\parallel},\text{term}}$ is smaller due to the alternating acceleration and deceleration. Note that $\dot{U}_{E_{\parallel}J_{\parallel},\text{term}}$ increases very weakly during $t = (13.5 - 15)\Omega_{ci}^{-1}$, and not at all where the curvature-type term is strongly enhanced. Off the center and near the separatrix, curvature-driven acceleration dominates even more than closer to the X-line (not shown here), while the parallel electric field acceleration decreases (see Fig. 1b).

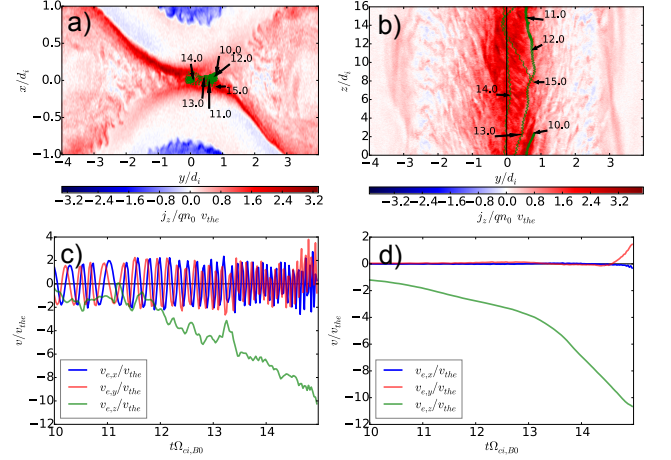


Figure 3. Projections of a typical energetic electron trajectory (green lines) to the a) plane $z = L_z/2$ and b) CS central plane $x = 0$. Subsequent electron positions are indicated by time marks in units of Ω_{ci}^{-1} . The colors depicts the current density j_z at $t_f = 15\Omega_{ci}^{-1}$. c) Evolution of the (four-)velocity components of the typical energetic electron (same as in a) and b)). d) Time history of the ensemble-averaged (four-)velocity components of the 10^4 most energetic electrons.

IV. Electron trajectories and spectrum

Figs. 3a)-b) depict projections of the trajectory of one self-consistently calculated by the PIC code strongly accelerated electron. Fig. 3c) shows the temporal evolution of its (four-)velocity components. Red and blue lines indicate gyration in the magnetic field, while the green line shows the different efficiencies of the electron acceleration during the two stages: a mild pre-acceleration mainly due to the parallel reconnection-electric field until $t \sim (12 - 13.4)\Omega_{ci}^{-1}$, and the nonlinear stage of reconnection, dominated by curvature-driven acceleration after the onset of the filamentation. This dominance starts earlier or later, depending on the motion phase of the electrons at the moment they enter the filaments. Fig. 3d) shows the time evolution of the average velocity components of the 10^4 most energetic electrons in a small domain near the X-line at $t \sim 15.0\Omega_{ci}^{-1}$. It confirms that the strongest acceleration takes place during the nonlinear stage of guide-field reconnection and after filamentation has started ($t \sim 13.4\Omega_{ci}^{-1}$). Out of the initially non-relativistic thermal distribution, now the fastest electrons

have reached mildly relativistic energies: the maximum four-velocity component $v_{e,z,max}$ corresponds to a particle speed of $0.74c$, i.e., to a relativistic Lorentz factor of $\gamma \sim 1.49$. This corresponds to an increase by two orders of magnitude of the electron kinetic energy.

The electron energization can be quantified by calculating an effective electric field ($E_{\text{eff}} = (m_e/e)a_{\text{eff}}$) which would cause the observed increase $a_{\text{eff}} = d\langle v_z \rangle / dt$ of the average velocity $\langle v_z \rangle$ of the 10^4 fastest electrons. In the pre-acceleration phase (up to $t \sim 13.4 \Omega_{ci}^{-1}$, see Fig. 3-d), a linear fit of $\langle v_z \rangle$ reveals $E_{\text{eff}} \sim 2.0 E_0$. At the nonlinear stage of reconnection, E_{eff} becomes, however, as large as $8.2 E_0$, which exceeds several times even the maximum value of E_{\parallel} near the X-line (about $1.5 E_0$).

Note that the periodic boundary conditions do not significantly affect the electron acceleration: even the most energetic electrons, with energies beyond the high energy end of the power-law part of the spectrum, cross the z -box boundaries maximum two-three times. Most electrons accelerated into the bulk of the power law part of the spectrum do not even cross the (periodic) z -boundaries once before they escape the acceleration region.

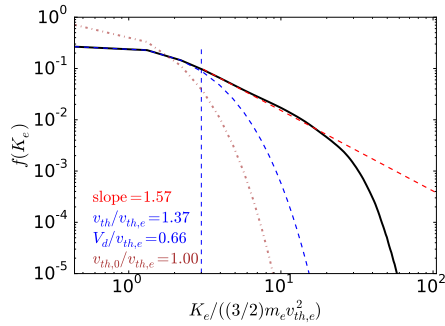


Figure 4. Electron energy spectrum at $t_f = 15 \Omega_{ci}^{-1}$. Brown dashed-dotted line: initial thermal distribution, blue dashed line: Maxwellian fit to the distribution, and red dashed line: power law fit to the energetic tail.

Fig. 4 shows the electron spectrum at the saturated nonlinear stage of reconnection ($t = t_f$), obtained for a region near the X-line extended $0.25d_i$ along x , $1.8d_i$ along y , and $16d_i$ along z . The Maxwellian fit of the thermal part of the spectrum indicates an electron heating by up to 40% above the initial temperature. The non-thermal tail of the electron distribution is best fitted by a power-law $f(K_e) = K_e^{-\alpha}$, with the electron kinetic energy $K_e = m_e c^2 (\gamma - 1)$. Simulations with more than 25 PPC reveal a spectral index $\alpha \sim 1.6$, independent on any further increase of PPC. The power-law part of the spectrum ranges over more than an order of magnitude above the initial thermal energy. There is an exponential cutoff at higher energies^{44,45}.

V. Conclusions and Discussion

We have shown that collisionless 3D guide-field magnetic reconnection in a non-relativistic electron-proton

plasma energizes electrons very efficiently due to its nonlinear evolution and filamentation, causing enhanced curvature-driven electron acceleration and resulting in a power law spectrum at single X-lines, even without island contraction (see, e.g., Drake *et al.*¹⁹, Dahlin, Drake, and Swisdak^{20,21}). The acceleration takes place in two-stages: the electrons are first pre-accelerated in the parallel reconnection electric-field, while during the nonlinear stage, curvature-driven acceleration in filamentary spatial structures dominates. The resulting electron energy distribution is characterized by heating and by a power-law with a spectral index of $\alpha \sim -1.6$. Such spectra were observed at reconnection sites by *in-situ* observations as well as in the solar corona, where electron spectra are deduced from hard X-ray emission of flares⁴⁶. Our findings do not intend to explain how the solar coronal plasma is heated to temperatures of millions of Kelvin, but to show how a power-law electron spectra is obtained out of a thermal distribution by guide-field magnetic reconnection. Those electrons might act, e.g., as seed particles required for Fermi acceleration processes in collisionless shocks.

Some features of this two-stage acceleration reminds aspects of first⁴⁷ and also second order Fermi acceleration⁴⁸. It is, however, neither characterized by bulk plasma flows nor by a stochastic electron motion. Instead it completely relies just on the magnetic-field curvature (second term in Eq. (1)). Fermi mechanisms also depend on elastic particles bounces⁴⁹, different from the dissipative processes present in our system.

The efficiency of the two-stage acceleration and the range of the power-law section in the spectrum increases with the length of the X-line. It is higher in thinner current sheets, in which streaming instabilities are stronger. The location of the high energy cutoff of the power-law distribution depends on the loss mechanism, mainly the electron escape from the reconnection region, controlled by the reconnection rate. After that, the energetic electrons are thermalized in the separatrixes and in the exhaust regions of reconnection. Although the pitch-angle scattering is weak in strong guide fields, the resulting thermalization softens the energy spectra with increasing distance from the X-line. Despite of the restriction of PIC-codes to simulate relatively small spatial domains, in particular compared to MHD-codes, the box sizes and number of PPC chosen here fully reproduced the two-stage electron acceleration and power-law energy spectrum formation by guide-field magnetic reconnection, which is controlled by dimensionless parameter ratios rather than by the absolute values of physical quantities⁵⁰.

Acknowledgments

We acknowledge the developers of the ACRONYM code (Verein zur Förderung kinetischer Plasmasimulationen e.V.). In particular, we are most grateful to Patrick Kilian for his helpful discussions and valuable comments. We acknowledge funding by the Max-Planck/Princeton

Center for Plasma Physics and PRACE (project prj.1602-008) for access to computational resources on the Beskow cluster at PDC/KTH, Sweden.

References

- ¹V. V. Zharkova, K. Arzner, A. O. Benz, P. Browning, C. Dauphin, A. G. Emslie, L. Fletcher, E. P. Kontar, G. Mann, M. Onofri, V. Petrosian, R. Turkmani, N. Vilmer, and L. Vlahos, “Recent Advances in Understanding Particle Acceleration Processes in Solar Flares,” *Space Sci. Rev.* **159**, 357–420 (2011), [arXiv:1110.2359](#).
- ²N. Vilmer, “Solar flares and energetic particles,” *Philos. Trans. R. Soc. A Math. Phys. Eng. Sci.* **370**, 3241–3268 (2012).
- ³J. L. Burch, R. B. Torbert, T. D. Phan, and et. al., “Electron-scale measurements of magnetic reconnection in space,” *Science* **352**, aaf2939 (2016).
- ⁴L.-J. Chen, M. Hesse, S. Wang, and et. al., “Electron energization and mixing observed by MMS in the vicinity of an electron diffusion region during magnetopause reconnection,” *Geophys. Res. Lett.* **43**, 6036–6043 (2016).
- ⁵M. Yamada, R. M. Kulsrud, and H. Ji, “Magnetic reconnection,” *Rev. Mod. Phys.* **82**, 603–664 (2010).
- ⁶M. Gordovskyy, P. K. Browning, and G. E. Vekstein, “Particle acceleration in a transient magnetic reconnection event,” *Astron. Astrophys.* **519**, A21 (2010).
- ⁷X. Zhou, J. Büchner, M. Bárta, W. Gan, and S. Liu, “Electron Acceleration By Cascading Reconnection In The Solar Corona. I. Magnetic Gradient And Curvature Drift Effects,” *Astrophys. J.* **815**, 6 (2015), [arXiv:1504.06486v1](#).
- ⁸L. Vlahos, H. Isliker, and F. Lepreti, “Particle Acceleration in an Evolving Network of Unstable Current Sheets,” *Astrophys. J.* **608**, 540–553 (2004), [arXiv:0402645 \[astro-ph\]](#).
- ⁹G. Kowal, E. M. de Gouveia Dal Pino, and A. Lazarian, “Particle Acceleration in Turbulence and Weakly Stochastic Reconnection,” *Phys. Rev. Lett.* **108**, 241102 (2012), [arXiv:1202.5256](#).
- ¹⁰S. Dalena, A. F. Rappazzo, P. Dmitruk, A. Greco, and W. H. Matthaeus, “Test-Particle Acceleration in a Hierarchical Three-Dimensional Turbulence Model,” *Astrophys. J.* **783**, 143 (2014).
- ¹¹J. Büchner and N. Elkina, “Anomalous resistivity of current-driven isothermal plasmas due to phase space structuring,” *Phys. Plasmas* **13**, 082304 (2006).
- ¹²M. Melzani, R. Walder, D. Folini, C. Winisdoer, and J. M. Favre, “The energetics of relativistic magnetic reconnection : ion-electron repartition and particle distribution hardness,” *Astron. Astrophys.* **570**, A112 (2014), [arXiv:1405.2938v1](#).
- ¹³F. Guo, X. Li, H. Li, W. Daughton, B. Zhang, N. Lloyd-Ronning, Y.-H. Liu, H. Zhang, and W. Deng, “Efficient Production of High-Energy Nonthermal Particles During Magnetic Reconnection in a Magnetically Dominated Ion–Electron Plasma,” *Astrophys. J.* **818**, L9 (2016).
- ¹⁴S. R. Tatorica, T. Abel, and F. Fiuza, “Non-Thermal Electron Energization from Magnetic Reconnection in Laser-Driven Plasmas,” *Phys. Rev. Lett.* **116**, 095003 (2016), [arXiv:1601.05845](#).
- ¹⁵S. Zenitani and M. Hoshino, “The Generation of Nonthermal Particles in the Relativistic Magnetic Reconnection of Pair Plasmas,” *Astrophys. J.* **562**, L63–L66 (2001).
- ¹⁶L. Sironi and A. Spitkovsky, “Relativistic reconnection: an efficient source of non-thermal particles,” *Astrophys. J.* **783**, L21 (2014), [arXiv:1401.5471](#).
- ¹⁷M. Hoshino, T. Mukai, T. Terasawa, and I. Shinohara, “Suprathermal electron acceleration in magnetic reconnection,” *J. Geophys. Res. Space Phys.* **106**, 25979–25997 (2001).
- ¹⁸J. Egedal, W. Daughton, and A. Le, “Large-scale electron acceleration by parallel electric fields during magnetic reconnection,” *Nat. Phys.* **8**, 321–324 (2012).
- ¹⁹J. F. Drake, M. Swisdak, H. Che, and M. A. Shay, “Electron acceleration from contracting magnetic islands during reconnection,” *Nature* **443**, 553–556 (2006).
- ²⁰J. T. Dahlin, J. F. Drake, and M. Swisdak, “The Mechanisms of Electron Heating and Acceleration during Magnetic Reconnection,” *Phys. Plasmas* **21**, 092304 (2014), [arXiv:1406.0831](#).
- ²¹J. T. Dahlin, J. F. Drake, and M. Swisdak, “Electron acceleration in three-dimensional magnetic reconnection with a guide field,” *Phys. Plasmas* **22**, 100704 (2015), [arXiv:1503.02218](#).
- ²²O. V. Khabarova and G. P. Zank, “Energetic Particles of keV–MeV Energies Observed near Reconnecting Current Sheets at 1 au,” *Astrophys. J.* **843**, 4 (2017).
- ²³M. Hoshino, “Stochastic Particle Acceleration in Multiple Magnetic Islands during Reconnection,” *Phys. Rev. Lett.* **108**, 135003 (2012), [arXiv:1201.0837](#).
- ²⁴J. F. Drake, M. Swisdak, and R. Fermo, “The Power-Law Spectra of Energetic Particles During Multi-Island Magnetic Reconnection,” *Astrophys. J.* **763**, L5 (2013).
- ²⁵P. Kilian, T. Burkart, and F. Spanier, “The Influence of the Mass Ratio on Particle Acceleration by the Filamentation Instability,” in *High Performance Computing in Science and Engineering '11*, edited by W. E. Nagel, D. B. Kröner, and M. M. Resch (Springer Berlin Heidelberg, Berlin, Heidelberg, 2012) pp. 5–13.
- ²⁶P. A. Muñoz, D. Told, P. Kilian, J. Büchner, and F. Jenko, “Gyrokinetic and kinetic particle-in-cell simulations of guide-field reconnection. I. Macroscopic effects of the electron flows,” *Phys. Plasmas* **22**, 082110 (2015), [arXiv:1504.01351](#).
- ²⁷J. May, J. Tonge, I. Ellis, W. B. Mori, F. Fiuza, R. A. Fonseca, L. O. Silva, and C. Ren, “Enhanced stopping of macro-particles in particle-in-cell simulations,” *Phys. Plasmas* **21**, 052703 (2014), [arXiv:1401.1198](#).
- ²⁸P. A. Muñoz and J. Büchner, “Kinetic turbulence in fast 3D collisionless guide-field magnetic reconnection,” *arXiv preprint*, [1705.01054](#) (2017), [arXiv:1705.01054](#).
- ²⁹J. F. Drake, M. Swisdak, C. Cattell, M. A. Shay, B. N. Rogers, and A. Zeiler, “Formation of Electron Holes and Particle Energization During Magnetic Reconnection,” *Science* **299**, 873–877 (2003).
- ³⁰H. Che, J. F. Drake, and M. Swisdak, “A current filamentation mechanism for breaking magnetic field lines during reconnection,” *Nature* **474**, 184–187 (2011).
- ³¹P. L. Pritchett, F. S. Mozer, and M. Wilber, “Intense perpendicular electric fields associated with three-dimensional magnetic reconnection at the subsolar magnetopause,” *J. Geophys. Res.* **117**, A06212 (2012).
- ³²V. Roytershteyn, W. Daughton, H. Karimabadi, and F. S. Mozer, “Influence of the Lower-Hybrid Drift Instability on Magnetic Reconnection in Asymmetric Configurations,” *Phys. Rev. Lett.* **108**, 185001 (2012).
- ³³Y. V. Khotyaintsev, A. Vaivads, M. André, M. Fujimoto, A. Retinò, and C. J. Owen, “Observations of Slow Electron Holes at a Magnetic Reconnection Site,” *Phys. Rev. Lett.* **105**, 165002 (2010).
- ³⁴R. E. Ergun, J. C. Holmes, K. A. Goodrich, and et. al., “Magnetospheric Multiscale observations of large-amplitude, parallel, electrostatic waves associated with magnetic reconnection at the magnetopause,” *Geophys. Res. Lett.* **43**, 5626–5634 (2016).
- ³⁵L. S. Shepherd and P. A. Cassak, “Guide field dependence of 3-D X-line spreading during collisionless magnetic reconnection,” *J. Geophys. Res. Space Phys.* **117**, A10101 (2012).
- ³⁶S. Dorfman, H. Ji, M. Yamada, J. Yoo, E. Lawrence, C. Myers, and T. D. Tharp, “Experimental observation of 3-D, impulsive reconnection events in a laboratory plasma,” *Phys. Plasmas* **21**, 012109 (2014).
- ³⁷J. D. Huba and L. I. Rudakov, “Three-dimensional Hall magnetic reconnection,” *Phys. Plasmas* **9**, 4435 (2002).
- ³⁸N. Jain and J. Büchner, “Spreading of magnetic reconnection by electron scale dispersive waves,” *arXiv preprint* (2016), [arXiv:1612.09242v1](#).
- ³⁹J. Büchner and J. Kuska, “Sausage mode instability of thin current sheets as a cause of magnetospheric substorms,” *Ann. Geophys.* **17**, 604–612 (1999).

- ⁴⁰G. Lapenta, D. Krauss-Varban, H. Karimabadi, J. D. Huba, L. I. Rudakov, and P. Ricci, “Kinetic simulations of x-line expansion in 3D reconnection,” *Geophys. Res. Lett.* **33**, L10102 (2006).
- ⁴¹J. Büchner and L. M. Zelenyi, “Regular and chaotic charged particle motion in magnetotail-like field reversals: 1. Basic theory of trapped motion,” *J. Geophys. Res.* **94**, 11821 (1989).
- ⁴²J. Büchner, M. Kuznetsova, and L. M. Zelenyi, “Sheared field tearing mode instability and creation of flux ropes in the Earth magnetotail,” *Geophys. Res. Lett.* **18**, 385–388 (1991).
- ⁴³T. G. Northrop, “Adiabatic charged-particle motion,” *Rev. Geophys.* **1**, 283 (1963).
- ⁴⁴N. Bessho and A. Bhattacharjee, “Fast Magnetic Reconnection and Particle Acceleration in Relativistic Low-density Electron-Positron Plasmas without Guide Field,” *Astrophys. J.* **750**, 129 (2012).
- ⁴⁵J. A. le Roux, G. P. Zank, G. M. Webb, and O. V. Khabarova, “Combining Diffusive Shock Acceleration With Acceleration By Contracting and Reconnecting Small-Scale Flux Ropes At Heliospheric Shocks,” *Astrophys. J.* **827**, 47 (2016).
- ⁴⁶G. D. Holman, L. Sui, R. A. Schwartz, and A. G. Emslie, “Electron Bremsstrahlung Hard X-Ray Spectra, Electron Distributions, and Energetics in the 2002 July 23 Solar Flare,” *Astrophys. J.* **595**, L97–L101 (2003).
- ⁴⁷E. Fermi, “On the Origin of the Cosmic Radiation,” *Phys. Rev.* **75**, 1169–1174 (1949).
- ⁴⁸L. Davis, “Modified Fermi Mechanism for the Acceleration of Cosmic Rays,” *Phys. Rev.* **101**, 351–358 (1956).
- ⁴⁹T. Pisokas, L. Vlahos, H. Isliker, V. Tsiolis, and A. Anastasiadis, “Stochastic Fermi Energization of Coronal Plasma during explosive magnetic energy release,” *Astrophys. J.* **835**, 1–30 (2017), [arXiv:1612.04246](https://arxiv.org/abs/1612.04246).
- ⁵⁰D. D. Ryutov, N. L. Kugland, H. S. Park, C. Plechaty, B. A. Remington, and J. S. Ross, “Basic scalings for collisionless-shock experiments in a plasma without pre-imposed magnetic field,” *Plasma Phys. Control. Fusion* **54**, 105021 (2012).